A Comparison of Water Vapor Measurements Made by Raman Lidar and Radiosondes

R. A. FERRARE,* S. H. MELFI,† D. N. WHITEMAN, K. D. EVANS,* F. J. SCHMIDLIN, AND D. O'C. STARR

NASA/Goddard Space Flight Center, Greenbelt, Maryland

(Manuscript received 18 November 1994, in final form 14 April 1995)

ABSTRACT

This paper examines the calibration characteristics of the NASA/GSFC Raman water vapor lidar during three field experiments that occurred between 1991 and 1993. The lidar water vapor profiles are calibrated using relative humidity profiles measured by AIR and Vaisala radiosondes. The lidar calibration computed using the AIR radiosonde, which uses a carbon hygristor to measure relative humidity, was 3%–5% higher than that computed using the Vaisala radiosonde, which uses a thin film capacitive element. These systematic differences were obtained for relative humidities above 30% and so cannot be explained by the known poor low relative humidity measurements associated with the carbon hygristor. The lidar calibration coefficient was found to vary by less than 1% over this period when determined using the Vaisala humidity data and by less than 5% when using the AIR humidity data. The differences between the lidar relative humidity profiles and those measured by these radiosondes are also examined. These lidar–radiosonde comparisons are used in combination with a numerical model of the lidar system to assess the altitude range of the GSFC lidar. The model results as well as the radiosonde comparisons indicate that for a lidar located at sea level measuring a typical midlatitude water vapor profile, the absolute error in relative humidity for a 10-min, 75-m resolution profile is less than 10% for altitudes below 8.5 km. Model results show that this maximum altitude can be extended to 10 km by increasing the averaging time and/or reducing the range resolution.

1. Introduction

Because of the important role water vapor plays in understanding diverse atmospheric processes such as radiative transfer, cloud formation, and energy transport, the requirement for frequent and accurate atmospheric water vapor measurements has become increasingly evident during recent years (Starr and Melfi 1991). Since water vapor is the dominant greenhouse gas, it will play an important role in any climate change scenario (Ramanathan 1988; Twomey 1991). Most climate models have found significant increases in water vapor in response to global warming; the resulting strong positive feedback associated with this increased water vapor has led models to show a 70% higher surface temperature response due to this feedback in addition to the direct effects of increased CO_2 (Arking 1991). Through its effect on the radiation budget, as well as its relationship with cirrus cloud formation, upper-tropospheric water vapor in particular has been identified as being an important variable in modeling any climate change associated with increased carbon dioxide (Lindzen 1990; Betts 1990).

Several measurement techniques have become available to address the need for improved water vapor measurements. These techniques include satellite (Larsen et al. 1993; Soden et al. 1994), microwave (England et al. 1992; Han et al. 1994; Wang et al. 1994), DIAL lidar (Ismail and Browell 1994), and Raman lidar (Melfi and Whiteman 1985; Vaughan et al. 1988; Melfi et al. 1989; Ansmann et al. 1992; Whiteman et al. 1992a). By virtue of its ability to provide both high spatial and temporal resolution measurements of water vapor throughout much of the troposphere during nighttime operations (Goldsmith et al. 1994) and in the surface layer during daytime operations (Eichinger et al. 1993), Raman lidar has emerged in recent years as a potential tool for providing the detailed water vapor profiles required for modeling the complicated processes discussed above. These detailed water vapor measurements, especially at upper-tropospheric levels, require understanding and quantifying the factors that limit the altitude range of the lidar measurements. This paper will address some of these factors and will attempt to explain how various atmospheric and system parameters influence these measurements.

Accurate and frequent assessments of the lidar water vapor calibration are also required before Raman lidar water vapor measurements can be used routinely in climate models. A common approach to calibrating these lidar systems relies on comparisons with coin-

* Hughes STX Corporation, Lanham, Maryland.
† University of Maryland Baltimore County, Baltimore, Maryland.

Corresponding author address: Richard A. Ferrare, NASA/Goddard Space Flight Center, Code 912, Greenbelt, MD 20771.

cident measurements of atmospheric water vapor (Melfi et al. 1989; Ansmann et al. 1992; Eichinger et al. 1993). Because of wide availability and relative ease of use, radiosondes have typically been used to provide calibration data. Over the past several years, we have been investigating how the water vapor profiles measured by the NASA/GSFC scanning Raman lidar compare with those measured by coincident radiosondes. These comparisons have been useful not only for monitoring the lidar performance but also for evaluating the capabilities and limitations of various radiosonde humidity sensors. In particular, we have used the lidar data to study the differences in the water vapor profiles measured by the carbon hygristor and thin-film capacitive elements, which are two common humidity-sensing devices used on radiosondes today.

In this paper, we briefly discuss the details of the GSFC Raman lidar and how it is used to measure water vapor profiles. We outline the method where coincident radiosonde data are used to calibrate the lidar water vapor measurements and present the calibration results obtained during three experiments between 1991 and 1993. We then compare the water vapor data measured by the lidar and radiosondes and discuss the differences among the instruments. Finally, the effects of instrumental and environmental factors on the maximum altitude of the Raman lidar water vapor retrievals are presented.

2. System

Melfi and Whiteman (1985), Melfi et al. (1989), England et al. (1992), and Koch et al. (1991) demonstrated the capability of a GSFC Raman lidar to provide high vertical resolution measurements of water vapor at night. These data have been used to study various meteorological processes and to assess the performance of other remote sensors that measure water vapor. The lidar system used for these studies went through several upgrades during its lifetime. The final system configuration and the techniques used to operate this system are described in Whiteman et al. (1992a). The experience gained through the modifications of this system was used to design and construct a new Raman lidar system, which was used to acquire the data described in this paper. A brief description of this new GSFC Raman lidar system follows. Additional information regarding this system is provided in Whiteman et al. (1992b).

The GSFC Raman lidar system uses a XeF laser to transmit light at 351 nm. A 0.76-m-diameter telescope collects the combined aerosol and molecular backscattered light at the laser wavelength, as well as Raman scattered light from water vapor (403 nm), nitrogen (383 nm), and oxygen (372 nm) molecules. A steerable elliptical flat (1.2 m × 0.8 m) provides full 180° horizon-to-horizon scan capability within a single-scan plane. Each wavelength is split into low and high sensitivity channels in order to measure the large range of return signals throughout the troposphere. Photomultiplier tubes operating in the photon-counting mode detect the backscattered radiation in all channels. In normal operation, data from more than 23 000 shots are recorded as 1-min profiles with a range resolution of 75 m. The data discussed in this paper were acquired at night. This was done to minimize interference from background skylight that interferes with the detection of the Raman signals, which are about three orders of magnitude weaker than the signal due to Rayleigh and Mie backscatter from molecules and aerosols.

Profiles of water vapor mixing ratio are computed from the ratio of the Raman water vapor to Raman nitrogen return signals. Since the laser beam is not fully within the field of view of the telescope for ranges less than about 1 km, a correction is applied to this ratio to account for this overlap function. This correction is obtained by placing a single, common nitrogen filter in these two channels so that both channels observe return signals at the same wavelength. The overlap function is then computed from the ratio of the return signals measured in these channels. Since both channels observe the same wavelength, this ratio does not depend on the atmospheric state and is therefore used to measure the overlap function. Application of this nitrogen filter calibration permits retrievals of water vapor profiles down to the lowest range gate acquired by the lidar, which is generally 100–200 m away from the lidar. Although scan data are not discussed here, water vapor profiles extending to within a few meters of the surface can be obtained by directing the laser beam at a nearly horizontal scan angle (Ferrare et al. 1993).

In addition to the overlap function correction, an additional correction is applied to account for the differential atmospheric transmission between the water vapor and nitrogen Raman wavelengths. This correction is mostly due to the wavelength dependence of Rayleigh scattering and increases with range away from the lidar, reaching approximately 7% at an altitude of 10 km. Although this correction generally can be computed with sufficient accuracy using density profiles from standard atmospheric models, the present method uses the density profiles computed from the coincident and collocated radiosondes used for the water vapor calibration and comparison studies that follow. For hazy conditions, an additional correction must be applied to account for the differential attenuation due to aerosol scattering. This correction, which can reach as high as 3%–4%, is computed from the aerosol extinction profiles measured simultaneously by the Raman lidar (Ansmann et al. 1990; Ferrare et al. 1992).

In addition to water vapor and aerosol extinction, profiles of the aerosol scattering ratio, defined as the ratio of total (aerosol plus molecular) to molecular scattering, are computed in a similar manner as water

vapor, except that the return signal at the laser wavelength is used in place of the water vapor signal. Thus, by forming this ratio, the Raman nitrogen return is used as a measure of molecular scattering, while the combined aerosol and molecular scattering is measured using the return signal at the laser wavelength. The aerosol scattering ratio is normalized to unity at an altitude between 6 and 10 km, where aerosol scattering is assumed to be negligible at 351 nm (Ferrare et al. 1992). As in the case of water vapor mixing ratio, an additional correction is applied to account for the differential atmospheric transmission between the laser and nitrogen Raman wavelengths. This correction is generally less than 10% and is computed in a similar manner to that described above for the water vapor mixing ratio. Further details regarding the computation of the aerosol scattering ratio are given by Ferrare et al. (1992). Since the scattering ratio increases abruptly when the laser beam strikes a cloud, these aerosol scattering ratio profiles are used to delineate any clouds that may be present. Clouds rapidly attenuate the laser beam so that water vapor retrievals are generally limited to altitudes below cloud base.

The standard errors for the water vapor and aerosol profiles are computed using Poisson statistics (i.e., the standard deviation is given by the square root of the total number of photon counts). Although these water vapor standard errors are comprised of the random errors in both the Raman water vapor and nitrogen return signals, the random error is given to a good approximation by the random error in the Raman water vapor signal. An example water vapor profile computed using a 10-min integration period, and 75-m vertical resolution is given in Fig. 1a using data acquired on 13 September 1993 at Wallops Island, Virginia. The methods used to calibrate the lidar data shown in this figure are discussed in section 4. The saturation mixing ratio curve also shown in this figure was computed from a coincident radiosonde temperature profile. The random error associated with the lidar water vapor mixing ratio is shown in Fig. 1b. The error decreases between 3 and 4 km, where the high-sensitivity channel data replace the low-sensitivity data. The relative humidity profile shown in Fig. 1c was computed using the lidar water vapor mixing ratio and the saturation mixing ratio profiles shown in Fig. 1a. The random error associated with the relative humidity profile is shown in Fig. 1d. Modeling results presented in section 7 show that increasing the averaging time and/or decreasing the spatial resolution can reduce the statistical uncertainty at any level.

3. Experimental data

The lidar and radiosonde data presented here were acquired during three experiments: FIRE Cirrus II [First ISCCP (International Satellite Cloud Climatology Project) Regional Experiment]/SPECTRE (Spectral Radiation Experiment) held near Coffeyville, Kansas, in November–December 1991; ATMIS II (Atmospheric Moisture Intercomparison Study) held at Wallops Island, Virginia, in July–August 1992; and CAMEX (Convection and Moisture Experiment) conducted at Wallops Island, Virginia, in September–October 1993. Radiosondes manufactured by the AIR (Atmospheric Instrumentation Research) and Vaisala corporations were used in each of the three field experiments. During the SPECTRE experiment, the AIR radiosondes were launched at the Raman lidar site by personnel from the NASA/GSFC/Wallops Flight Facility, while the Vaisala radiosondes, which were part of the NCAR Cross-chain Loran Atmospheric Sounding System (CLASS), were launched approximately 0.5 km northwest of the lidar site. Separate balloons carrying these packages were generally flown 1–3 h apart so that direct comparisons between these sondes are not possible. However, the Raman lidar operated continuously during the sonde observations and can therefore be used to compare these different radiosonde measurements. During the SPECTRE experiment, there were 24 Raman lidar–AIR radiosonde coincident measurements and 17 Raman lidar–Vaisala radiosonde coincident measurements.

The ATMIS II experiment was a continuation of the previous ATMIS I experiment, which was also performed at Wallops Island, Virginia, during April 1989 and during which water vapor measurements made by the Raman lidar, radiosondes, and ground-based microwave radiometers were compared (England et al. 1992; England et al. 1993). ATMIS II employed similar sensors except that an airborne millimeter-wave imaging radiometer flown on an ER-2 replaced the ground-based microwave radiometer (Wang et al. 1995). During ATMIS II, the AIR and Vaisala sensors were carried aloft by the same balloon so that direct comparisons could be made between the radiosondes as well as with the lidar. These radiosondes were launched approximately 3 km east of the lidar site at a site approximately 200 m from the ocean. On five nights between 29 July and 6 August there were 16 radiosonde flights coincident with the lidar measurements; these radiosondes were generally launched at 2100, 0000, 0300, and 0600 local time.

The CAMEX experiment was designed to measure the atmospheric thermodynamic, electrical, and cloud fields associated with convection, as well as to measure high-resolution profiles of temperature and moisture (Griffin et al. 1994). CAMEX also took place at Wallops Flight Facility and included several airborne instruments mounted on the ER-2 aircraft as well as the scanning Raman lidar and radiosondes. Like ATMIS II, AIR and Vaisala sensors were flown simultaneously on several balloons so that direct comparisons could be made among the various water vapor sensors. These

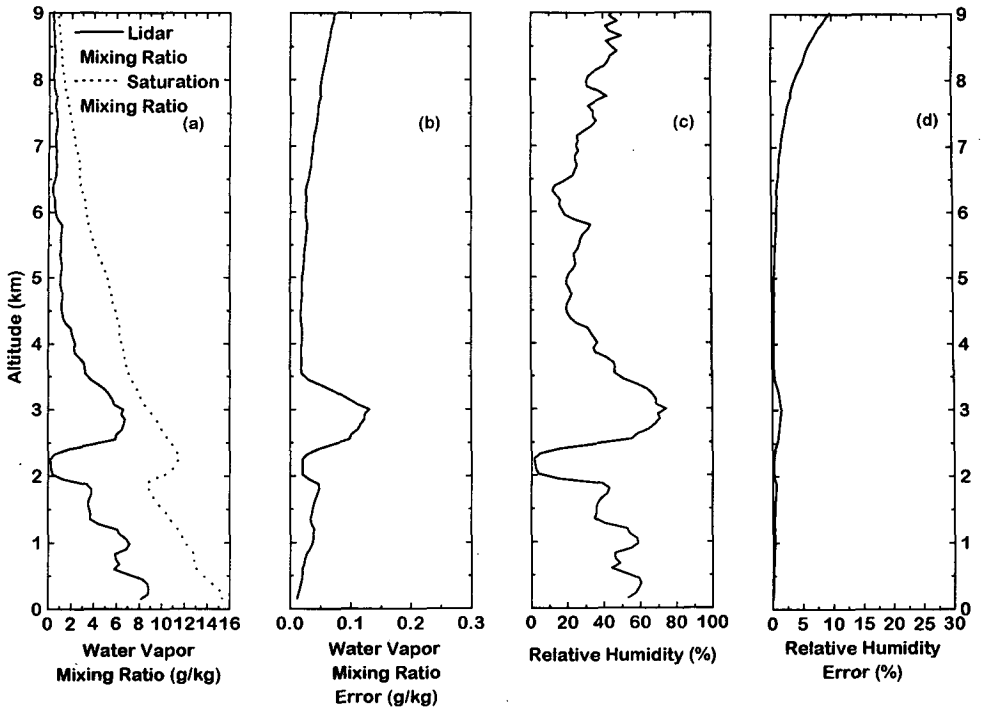

FIG. 1. (a) A 10-min, 75-m vertical resolution lidar water vapor profile acquired at 0237 UTC 13 September 1993 at Wallops Island, Virginia. (b) Random error (precision) of water vapor profile shown in (a). The decrease in error between 3 and 4 km is due to the transition from low to high sensitivity channels. (c) Relative humidity profile corresponding to lidar mixing ratio profile shown in (a). (d) Random error (precision) of relative humidity profile shown in (c).

radiosondes were generally launched at 1800, 2100, 0000, and 0300 local time at a coastal site about 3 km east of the lidar. During the period between 13 September through 6 October there were 13 AIR–lidar comparisons and 18 Vaisala–lidar comparisons. In addition, personnel from the University of Wisconsin–Madison launched Vaisala radiosondes that used the CLASS data acquisition system. These sondes were released from a location approximately 2 km west of the lidar site generally within 10–15 min of the times listed above. There were 22 Vaisala–lidar intercomparisons available using this second set of radiosondes.

The AIR and Vaisala radiosondes use different types of moisture sensors. The AIR radiosondes carried carbon hygristor moisture elements manufactured by the VIZ corporation, while the Vaisala sondes carried the Humicap thin-film capacitive element sensor. The carbon hygristor elements are the same as those currently used operationally by the National Weather Service. The carbon hygristor element has a stated accuracy ranging from ±5% (for relative humidities 20%–90%) to 7% (for relative humidities 0%–20% and 90%–100%), while the precision is stated to be ±3% (root-mean-square) (Larsen et al. 1993). The stated accuracy of the Vaisala sensors is 2%–3% over the entire range of relative humidities with a precision of 2% (Larsen et al. 1993). Pratt (1985) found that for a VIZ carbon hygristor element, the response time for normal balloon ascent rates gives an approximate vertical resolution of 150 m for temperatures above −30°C and even larger values for colder temperatures. Schmidlin (1988) found that the response time for the Vaisala sensor is as good as or better than the carbon hygristor. The radiosonde data used in this study showed considerable variability on scales smaller than the 150 m listed above.

The performance numbers given above for the carbon hygristor element do not fully characterize this sensor as several recent studies (Melfi et al. 1989; Wade and Wolfe 1989; Elliot and Gaffen 1991; Garand 1992; Wade 1994) have documented the problems associated with measurements of low relative humidities by these carbon hygristor elements. The comparisons presented in the following sections will also clearly show these low-relative-humidity sensing problems. While the Humicap capacitive sensor has provided more representative measurements than the carbon hygristor element in low relative humidity conditions (Wade and Wolfe 1989; Wade 1994), the following sections will demonstrate that *systematic differences exist between these two moisture-sensing elements for nearly all relative humidities.*

4. Lidar calibration procedure

As discussed in section 2, profiles of water vapor mixing ratio are computed from the ratio of Raman water vapor to Raman nitrogen return signals. Whiteman et al. (1992a) show that a single calibration constant is used to convert these lidar ratios into water vapor mixing ratios expressed as the mass of water vapor divided by the mass of dry air. Two different methods have been used to obtain this calibration constant. One approach requires accurate knowledge of the optical transmission characteristics and the Raman scattering cross section of water vapor relative to that of nitrogen. Vaughan et al. (1988) used this approach to compute calibration values with a precision of 12%. Because of the difficulty in reducing this figure due to uncertainties in the Raman cross sections and in determining the optical transmission characteristics of the entire lidar detection system, we have adopted a second approach where many lidar profiles are compared with simultaneous and collocated radiosonde measurements of water vapor.

Although obtaining a single water vapor calibration constant by comparing the lidar water vapor mixing ratio profile data with coincident radiosonde water vapor profiles would appear to be a straightforward exercise, actual radiosonde data show that considerable differences often occur between the radiosonde humidity measurements. Figure 2 shows one example of these differences. The relative humidity profiles measured by AIR and Vaisala sensors carried aloft by the same balloon during a flight on 30 July 1992 during the ATMIS II experiment are shown. A 10-min, 75-m resolution lidar water vapor profile acquired simultaneously with these radiosonde profiles is also shown. The lidar relative humidity profile was computed using the lidar water vapor mixing ratio profile and the radiosonde temperature profile. The calibration constant used to obtain the lidar water vapor mixing ratio profile is discussed in the next section, and the computation of the lidar relative humidity profile is discussed in section 6. The poor low-relative-humidity measurements associated with the carbon hygristor used on the AIR sensor, while evident for altitudes above 2.5 km, are clearly not sufficient to explain the differences between the two radiosondes below 2.5 km. Unfortunately, differences between radiosonde water vapor profiles like those shown in Fig. 2 are not uncommon. Because it is not clear which radiosonde sensor provides the better measurement of water vapor under all conditions, we have computed a single, range-independent lidar calibration constant using each (AIR and Vaisala) radiosonde during the three experiment periods.

During the SPECTRE experiment (November–December 1991), there were a total of 41 radiosondes launched coincidentally with the lidar measurements; of these, 24 were AIR sondes, while 17 were Vaisala

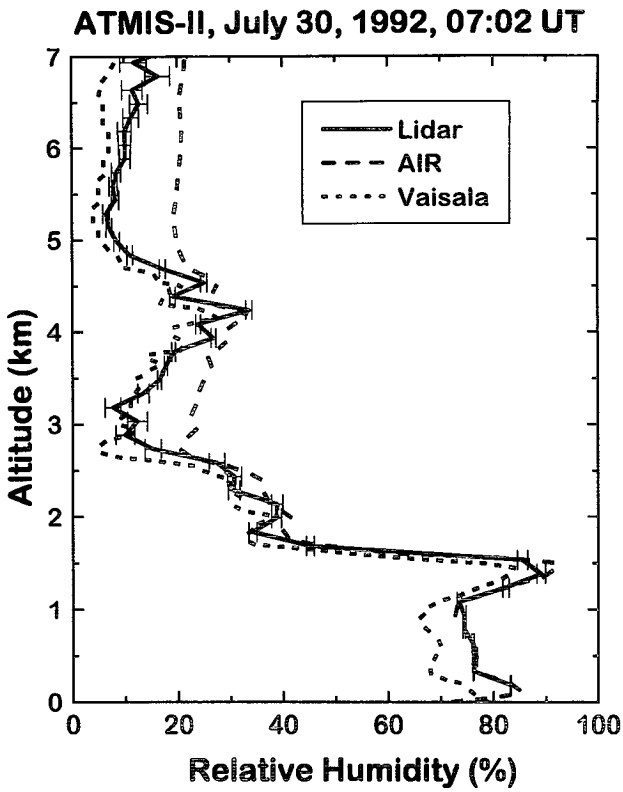

FIG. 2. AIR and Vaisala radiosonde and lidar relative humidity profiles acquired at 0702 UTC 30 July 1992 at Wallops Island, Virginia. Both radiosondes were carried aloft by the same balloon. The lidar profile is a 10-min average beginning at the time of radiosonde launch.

sondes. As discussed previously, these sondes were not flown simultaneously, so a direct AIR–Vaisala comparison is not possible. Each of these 41 radiosondes was used independently to compute, for that particular flight, a single altitude-independent calibration constant to convert lidar data to water vapor mixing ratio. The radiosonde data were first low-pass filtered using a "nearly equal ripple" filter (Kaiser and Reed 1977) to an equivalent 75-m resolution to match the lidar resolution. The 10-min average lidar profiles were used in each comparison; these averages were computed starting from the time of radiosonde launch to 10 min after launch. During this time, the radiosonde normally ascends to an altitude of about 3 km (about 700 mb). The importance of comparing coincident and collocated radiosonde data must be emphasized. The high temporal and spatial resolution lidar water vapor profiles have consistently demonstrated the highly variable nature of atmospheric water vapor (Melfi et al. 1989). Differences of 50% between the lidar and radiosonde water vapor measurements can occur if the two measurements differ by more than 20–30 min or 20–30 km. Lidar data between altitudes 0.185 and 8.0 km

were used in the calibration regression. The maximum altitude will be examined in more detail in section 7. If clouds were present, no lidar data were used above cloud base so that in some cases the maximum altitude was less than 8 km. Cloud-base altitudes were easily determined from the lidar aerosol-scattering ratios measured simultaneously with the water vapor mixing ratios.

In the regression procedures used to calibrate the lidar ratios to radiosonde water vapor mixing ratios, radiosonde data for relative humidities below 30% were excluded from the comparison. This limit was imposed because of the problems the carbon hygristor has in accurately reporting water vapor for low relative humidities (Wade 1994). Although 20% is the relative humidity limit most often associated with this problem, examination of several coincident AIR and Vaisala relative humidity profiles during the ATMIS II and CAMEX experiments showed that the AIR humidity profiles often reached a lower limit well above 20%. The reason for the variability in this lower limit is not known at this time. The 30% relative humidity lower limit for radiosonde data used in the calibration procedure was applied to the Vaisala data as well so that the lidar-calibration results from both radiosonde humidity datasets could be compared directly. If the 30% relative humidity limit is removed so that all radiosonde data are used in the calibration, the Vaisala calibration values change by less than 1%. Relative humidity effects will be discussed in more detail in section 6. If all data were used, approximately 100 altitude levels would be available for use in the least squares regression to determine each of the 41 potential calibration constants for FIRE II/SPECTRE. However, a typical radiosonde–lidar comparison had considerably fewer levels due to this 30% relative humidity restriction and the requirement to avoid clouds. For the SPECTRE comparison dataset, the minimum, average, and maximum number of points used in any of the 41 regressions were 11, 45, and 104, respectively.

The procedures used to calibrate the lidar using radiosonde data from the ATMIS II and CAMEX experiments are similar to those described above. During ATMIS II, there were a total of 16 AIR and 16 Vaisala radiosondes available for comparison with the lidar; 15 of the balloons launched during this experiment carried both radiosonde packages simultaneously so that direct comparisons between the radiosonde sensors could be made. Although the scanning ability of the GSFC Raman lidar was used periodically during ATMIS II, all of the lidar data used here were acquired when the lidar was pointed vertically. During CAMEX, there were a total of 13 AIR and 18 Vaisala WFF (Wallops Flight Facility) radiosondes available for comparison; 13 of the balloons carried both the AIR and Vaisala packages so that again direct comparisons could be made between the two sensors. The additional 22 Vaisala sondes launched by UW personnel about 5 km west of the first balloon site were nearly coincident with these WFF radiosondes. The scan mode of lidar data acquisition was used extensively during CAMEX. In this mode, data were sequentially acquired from a series of angles throughout the night. The lidar data used in the following calibration and comparison procedures were computed by summing five 1-min profiles acquired along the vertical. Because the vertical data were interspersed with the other scan angles, summing consecutive vertical profiles took slightly longer than during the previous two experiments. Thus, the lidar profiles used during the CAMEX experiment typically consisted of 5-min averages acquired over a period of about 15 min.

5. Calibration results

Calibration constants were computed between the individual lidar profiles and each coincident radiosonde measurement following the procedures outlined above. A single calibration constant corresponding to each sensor type (AIR and Vaisala) was then computed for each experimental period by averaging the individual calibration constants. These average calibration constants, shown in Fig. 3, are the multiplicative constants required to convert the lidar ratios to water vapor mixing ratio in units of grams of water vapor per kilogram of dry air. In Fig. 3c, Vaisala 1 represents the Vaisala sondes launched by WFF personnel, while Vaisala 2 represents those launched by UW personnel. Within each experiment period, no significant trends were observed since the calibration constants were randomly distributed. The calibration constants computed using only AIR sonde data were about 5% higher than those computed using only Vaisala data during the SPECTRE and CAMEX experiments and approximately 9% higher during the ATMIS II experiment. As will be shown later, a similar trend was observed when all AIR and Vaisala relative humidity measurements, not just those obtained during lidar observations, were compared. In addition, these results are for relative humidities above 30%, so that this bias is apparently unrelated to the low relative humidity measurements associated with the carbon hygristor element on the AIR sonde.

The data presented in Fig. 3 indicate that over this 2-yr period, the lidar calibration constant varied by less than 1% when computed using Vaisala radiosonde data and less than 5% when computed using AIR radiosonde data. This remarkable stability is surprising considering changes were made to the system during routine maintenance and periodic tests. An estimate of the variability of the radiosonde data can also be seen from the error bars shown in Fig. 3. Sonde-to-sonde measurements of water vapor can easily vary by 5% regardless of the type of moisture-sensing element.

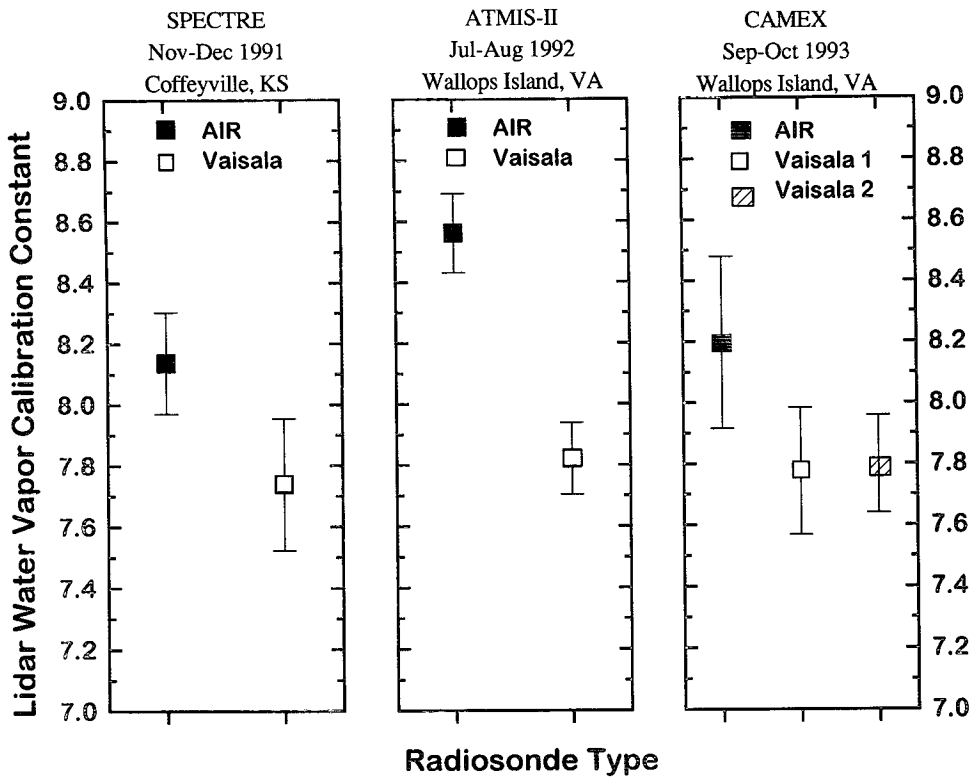

FIG. 3. Lidar calibration constants obtained by comparisons with AIR and Vaisala radiosondes. Two separate Vaisala radiosondes were launched during the CAMEX experiment at locations separated by about 5 km. Error bars represent standard deviations.

While the lidar data shown in Fig. 3 indicate systematic differences in moisture measurements existed between these two radiosonde sensors, it is not clear which radiosonde provides a better measurement of water vapor for relative humidities above 30%. Comparison data shown in the next section clearly demonstrate the limitations associated with the carbon hygristor for measuring moisture in dry conditions. Because of this inability to resolve which calibration estimate is more accurate, a single calibration constant for each experimental period was then computed by simply averaging all (AIR and Vaisala) calibration values together. The resulting calibration values for these periods are 7.97, 8.19, and 7.89 for the SPECTRE, ATMIS II, and CAMEX experiments, respectively.

The lidar water vapor measurements were compared with measurements made by other sensors in an attempt to resolve this uncertainty in the lidar calibration. For example, the lidar moisture measurements obtained during the SPECTRE experiment have been compared with those provided by a microwave radiometer as well as by the GOES 6.7-μm channel. Because the broad weighting functions associated with these other sensors generally prevent these passive devices from providing detailed water vapor profiles, the lidar mixing ratio profile data were integrated in the vertical to match the altitude ranges measured by these two sensors. Han et al. (1994) found a root-mean-square difference of 0.03 cm and a bias of 0 cm between precipitable water amounts computed from the lidar data and those measured by the collocated three-channel microwave radiometer operated by the NOAA Environmental Technology Laboratory during the FIRE II/SPECTRE experiments. Coincident radiosonde measurements were used to estimate the nondiagonal covariance matrix used to construct the retrieval coefficients in the microwave radiometer precipitable water measurements. The comparison with the microwave radiometer suggests that the best lidar calibration does lie between the values provided by the Vaisala and AIR radiosondes.

Soden et al. (1994) compared upper-tropospheric water vapor amounts derived from the GOES 6.7-μm channel with those measured by the Raman lidar and the Vaisala radiosondes during the SPECTRE experiment. This dataset included several of the lidar–radiosonde intercomparison profiles used in this study. GOES measurements of upper-tropospheric relative humidity agreed slightly better with the lidar observations than with the Vaisala observations. Soden et

al. (1994) found that the Vaisala sondes slightly underestimated the upper-tropospheric water vapor when compared to both the lidar and GOES-7 estimates.

Lidar and radiosonde water vapor profiles measured during the ATMIS II experiment were also used to compute microwave brightness temperatures at the six frequencies measured by the airborne millimeter-wave imaging radiometer (MIR). Comparisons between the measured and computed brightness temperatures showed differences generally less than 2–3 K for those temperatures computed using lidar and Vaisala moisture profiles but increased to about 10 K for those computed using AIR moisture profiles (Wang et al. 1995; Jackson and Gasiewski 1994). This large difference between the measured brightness temperatures and those computed using the AIR profiles was attributed to the problems associated with the carbon hygristor in reporting relative humidities below 20%.

As just discussed, the integrated column precipitable water vapor amounts measured by other sensors have compared well with the values measured by the Raman lidar. However, these sensors have not been able to provide sufficient information to significantly reduce the uncertainty in the lidar calibration introduced by using the two radiosondes. Because of these radiosonde differences, the question arises as to whether other sensors that measure detailed profiles of water vapor could be used to check the lidar calibration. As one attempt, water vapor data acquired from the NCAR King Air during the SPECTRE experiment in 1991 were examined. This aircraft flew spiral ascent and descent patterns above the lidar site on the nights of 26 November and 4 December coincident with lidar operations. Several moisture-sensing instruments were onboard the aircraft. Two chilled-mirror dewpoint hygrometers were used; a General Eastern model was mounted above the fuselage, while an EG&G hygrometer was mounted below the fuselage. These instruments have dewpoint accuracies of about 0.5°–2.0°C depending on temperature; these values were based on comparisons with simultaneous measurements of air temperature during those FIRE II flight periods that contained liquid water (A. Heymsfield 1994, private communication). A 2°C error in dewpoint would produce an error of about 16% in water vapor mixing ratio at a pressure of 900 mb and a temperature of −4°C. In addition, a cryogenic frost-point hygrometer was used to measure water vapor for temperatures below −20°C (Heymsfield and Miloshevich 1993). At these temperatures, the instrument has an accuracy of about 1°C in frost point (Heymsfield and Miloshevich 1995).

Since the aircraft ascent and descent patterns each took about one hour to complete as the plane flew between the surface and 9 km, the procedure used to compare lidar and aircraft moisture measurements was modified to minimize potential differences between the lidar and aircraft water vapor measurements that may have occurred during these 1-h periods. Rather than summing all 60 min of lidar data coincident with the aircraft ascent and descent patterns, the lidar data closest in time at each aircraft reporting altitude were used to construct composite profiles. Examples of these lidar and aircraft water vapor mixing ratio measurements are shown for the aircraft ascent (Fig. 4a) and descent (Fig. 4b) on 4 December. Data from the cryogenic frost-point hygrometer are shown only for altitudes above 5.3 km where temperatures were colder than −20°C.

While the agreement is excellent among the various sensors during the aircraft descent, the aircraft measurements are all 5%–15% lower than the lidar measurements in the lowest 3 km during aircraft ascent. A similar pattern between lidar measurements and those measured during aircraft ascent and descent was observed on 26 November. The reason for the different behavior between aircraft ascent and descent is currently unclear. Dewpoint measurements should not be affected by the angle of attack of the aircraft. Water vapor mixing ratio is a function of dewpoint (or frost point) and pressure only and is therefore not affected by possible temperature measurement errors. Below 3 km, the spiral flight pattern indicated that the aircraft acquired data at all azimuth angles within 10 km of the lidar site. Thus, it is difficult to visualize how spatial variations in the water vapor field could have produced systematic differences between the lidar and aircraft measurements. These differences are not expected to be caused by hysteresis in the chilled mirror instruments since the response times of these instruments are generally less than a few seconds (Spyers-Duran 1994, private communication). An AIR radiosonde launched at the lidar site at 0158 UTC (between aircraft ascent and descent) showed excellent agreement with the lidar water vapor measurements.

Another potential method to calibrate the lidar involves comparing the lidar measurements with data acquired by surface-based water vapor instruments. The scanning capability of the GSFC Raman lidar permits the lidar to acquire data pointing nearly horizontally so that data can be acquired from horizon to horizon in a single scan plane. By proper orientation, these nearly horizontal data can be compared with surface- and/or tower-based instrumentation. While this method has the advantage of using a surface-based instrument whose calibration characteristics are presumably well known, it has the disadvantage that lidar data at only a single range bin are used. Therefore, the behavior of the lidar water vapor calibration as a function of range cannot be examined. We intend to pursue this method in future experiments where feasible.

6. Lidar–radiosonde comparisons

The lidar calibration results discussed in the previous section demonstrated that the water vapor profiles

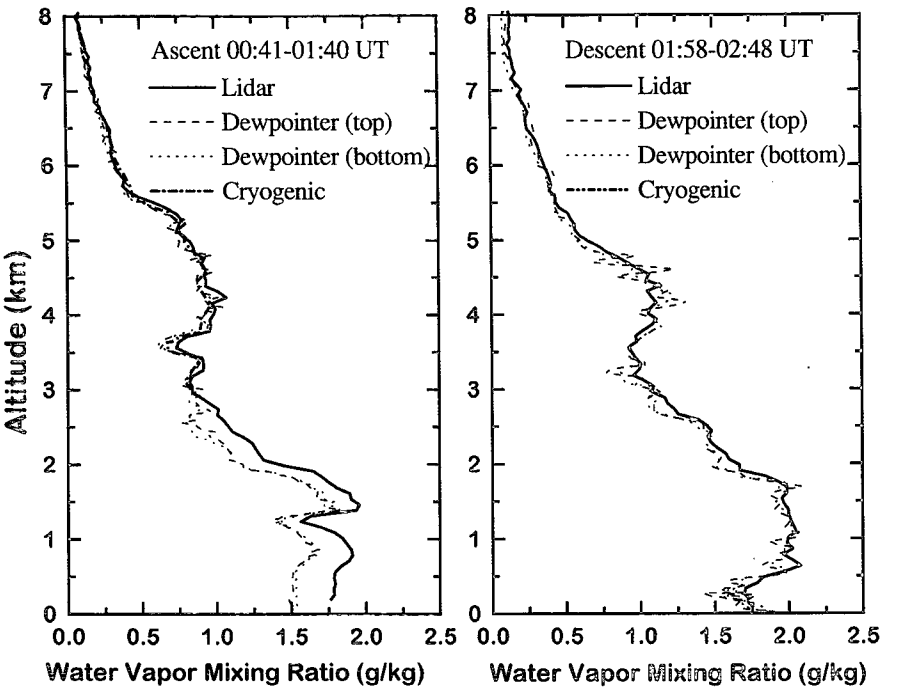

FIG. 4. (a) Lidar and aircraft water vapor profiles measured between 0041 and 0140 UTC 4 December 1991 near Coffeyville, Kansas. Dewpoint hygrometers were mounted both above and below the NCAR King Air aircraft. Data were acquired during aircraft ascent. (b) Same as (a) except data acquired during aircraft descent between 0158 and 0248 UTC.

measured by the AIR and Vaisala radiosondes exhibit systematic differences. In this section we investigate the radiosonde measurements of relative humidity and compare these with the lidar measurements. Since the conversion of water vapor mixing ratio to relative humidity requires coincident measurements of pressure and temperature, the lidar measurements of water vapor mixing ratio were converted to relative humidity using the radiosonde pressure and temperature profiles. While vibrational Raman lidar systems such as the GSFC lidar have measured temperature profiles in the upper troposphere and lower stratosphere (Keckhut et al. 1990; Ferrare et al. 1990; K. Evans, S. Melfi, R. Ferrare, and D. Whiteman 1994, private communication), aerosol attenuation prohibits the use of this technique in the lower troposphere. For these mixing ratio to relative humidity conversions, the Goff–Gratch formula relating temperature and saturation vapor pressures was used (List 1949). This method is expected to give values within 2% for the temperatures used in the current study (Elliot and Gaffen 1991). In those cases where both AIR and Vaisala radiosondes were available, the AIR pressure and temperature profiles were used.

Since errors in the radiosonde temperature profiles can obviously lead to erroneous lidar relative humidities, we also examined the temperatures measured by both radiosondes. The temperatures from both radiosondes launched on the same balloon were compared as a function of time after launch rather than pressure or altitude in order to reduce any registration errors. The temperatures were interpolated to regularly spaced 12-s intervals for the entire radiosonde flights. Figure 5 shows the AIR–Vaisala temperature differences for those sondes carried by the same balloon during the ATMIS II and CAMEX experiments. The radiosondes normally ascended to 10 km in about 30 min. Temperature differences between the AIR and Vaisala shown in Fig. 5 were computed by averaging the results over 4-min intervals in order to increase the statistical significance of the results. These temperature comparisons were computed using 16 coincident AIR–Vaisala flights flown during lidar operations during ATMIS II (1992) and 13 coincident AIR–Vaisala flights flown during lidar operations during CAMEX (1993). Figure 5 shows that temperature differences between the two sondes were generally less than 0.5°C, with AIR temperatures slightly cooler than the Vaisala readings for tropospheric temperature measurements. These measurements were acquired at night during lidar operations so that solar radiation effects should not be observed (Schmidlin 1988). The slightly cooler temperatures recorded by the AIR sonde during nighttime flights agree with the trends reported by Schmidlin (1988) for a series of comparison flights during early 1985 at Wallops Island, Virginia. The effect of using

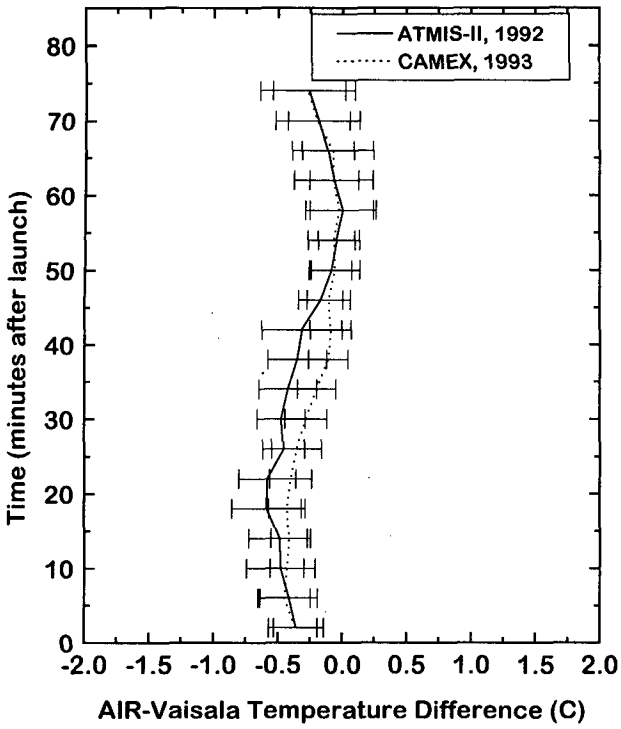

FIG. 5. AIR–Vaisala temperature differences obtained from 16 coincident flights during ATMIS II and 13 coincident flights during CAMEX. Time is expressed as minutes after radiosonde launch. Temperature differences were averaged over 4-min intervals to increase statistical significance.

the slightly lower AIR temperature profiles in conjunction with the lidar water vapor mixing ratios will produce relative humidities that are generally less than 2% higher than those that would be computed using Vaisala temperature profiles.

The distribution of relative humidities computed from the lidar water vapor mixing ratios and the radiosonde temperatures are shown in Fig. 6a for the ATMIS II experiment and Fig. 6b for the CAMEX experiment. The data plotted in these figures correspond to the 75-m altitude spacing of the lidar profiles for altitudes between 0.185 and 8 km. There were 15 simultaneous AIR–Vaisala flights for the ATMIS II experiment and 13 for the CAMEX experiment. Since the AIR and Vaisala radiosondes were not flown simultaneously during SPECTRE, a similar graph for this experiment is not possible. The inability of the AIR sondes to report low relative humidity values is clearly evident from Fig. 6 since the AIR sonde reported no humidities below 10%, while the Vaisala and lidar reported 40% and 35% of the measurements below 10%, respectively, during ATMIS II and 15% and 17%, respectively, during CAMEX.

The problems associated with the measurement of low relative humidities by the radiosonde carbon hygristor sensors as shown in Fig. 6 have been observed and periodically documented since the National Weather Service began routinely using these sensors in 1965. Brousaides and Morrissey (1971) noted this problem when comparing the National Weather Service (NWS) and Department of Defense (DOD) radiosonde sensor performance. After comparing the performance of the military and NWS versions of these sensors and finding significant differences between the versions, Brousaides (1975) suggested revising the data reduction methods used for the NWS radiosondes when relative humidities below 20% are desired. These problems became readily apparent when comparing these radiosonde measurements with those provided by microwave radiometer (Westwater et al. 1989; England et al. 1992), Raman lidar (Melfi et al. 1989), and SAGE II satellite (Larsen et al. 1994), as well as with the radiosonde measurements made in other countries (Garand et al. 1992). Wade and Wolfe (1989) and Wade (1991, 1994) claim that the low relative humidity reporting problems stem mainly from the use of two sets of coefficients used to convert the resistance values to relative humidities. One set of coefficients is used

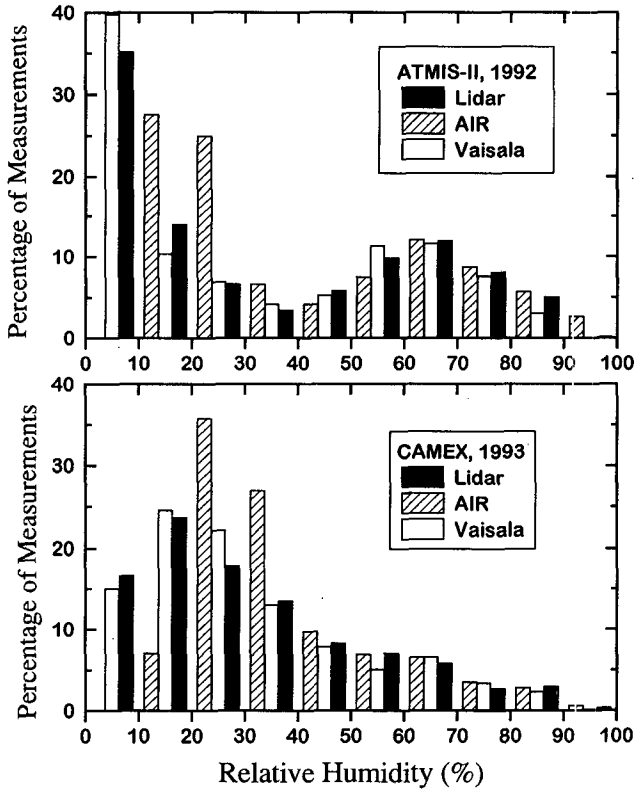

FIG. 6. Distribution of relative humidities measured by the lidar and radiosondes during the ATMIS II (top) and CAMEX (bottom) experiments. These data correspond to 75-m vertical resolution data for altitudes between 0.185 and 8.0 km. There were 15 coincident comparisons among all three systems during ATMIS II and 13 during CAMEX.

for relative humidities above 20%, while the second set is used for values below 20%. Wade (1994) states that using the first set of coefficients exclusively should in fact give a closer match to the actual carbon hygristor sensor response at low relative humidities. At the time of this writing, we cannot confirm this but plan to reprocess selected radiosondes launched during the CAMEX experiment with the recommended coefficients to evaluate this hypothesis.

The differences among the relative humidities measured by the lidar, AIR, and Vaisala sensors were first examined as a function of relative humidity. Figure 7 shows the difference between the lidar and radiosonde relative humidities for each of the three experiments. The mean differences were computed for lidar relative humidities between 0% and 100% in increments of 10%. As discussed in section 5, the calibration value for each of the three periods was found by averaging the Vaisala and AIR results together. Therefore, the values shown in Fig. 7 are expected to be positive (lidar moister) for the Vaisala comparison and negative (lidar drier) for the AIR comparison. The low relative humidity reporting problem of the AIR is immediately obvious and is apparent for relative humidities below about 30%. The bias between the lidar and Vaisala data is generally less than ±5%. The ATMIS II and CAMEX datasets show the lidar–Vaisala radiosonde bias to be relatively constant with relative humidity, although a small decrease in the bias can be seen for relative humidities below about 30%–40%. A decrease in bias with decreasing relative humidity is present for the SPECTRE data. The reason for this decrease is not clear, although it should be noted that the relative humidities present in the SPECTRE dataset were lower than those present during the other two campaigns. All data show the AIR radiosonde humidities are about 3%–6% higher than those reported by the Vaisala sonde for humidities above 30%. Significance tests computed using the Student's t distribution indicate that, with the exception of relative humidities above 80% during the SPECTRE and ATMIS II campaigns, these differences are significant at the 90% confidence level. These differences between sonde relative humidities can be more easily seen in Fig. 8. In this figure are shown the relative humidity difference (AIR minus Vaisala) as a function of Vaisala relative humidity using all coincident radiosondes launched during both ATMIS II and CAMEX experiments. These data include 15 simultaneous AIR–Vaisala launches that occurred during ATMIS II and the 24 that occurred during CAMEX; these data are for radiosondes launched in the daytime as well as nighttime and therefore include additional data acquired outside of lidar observations and not included in Fig. 7. Here again the 3%–6% difference between the AIR and Vaisala sonde can be seen. Significance tests indicate that these differences are sig-

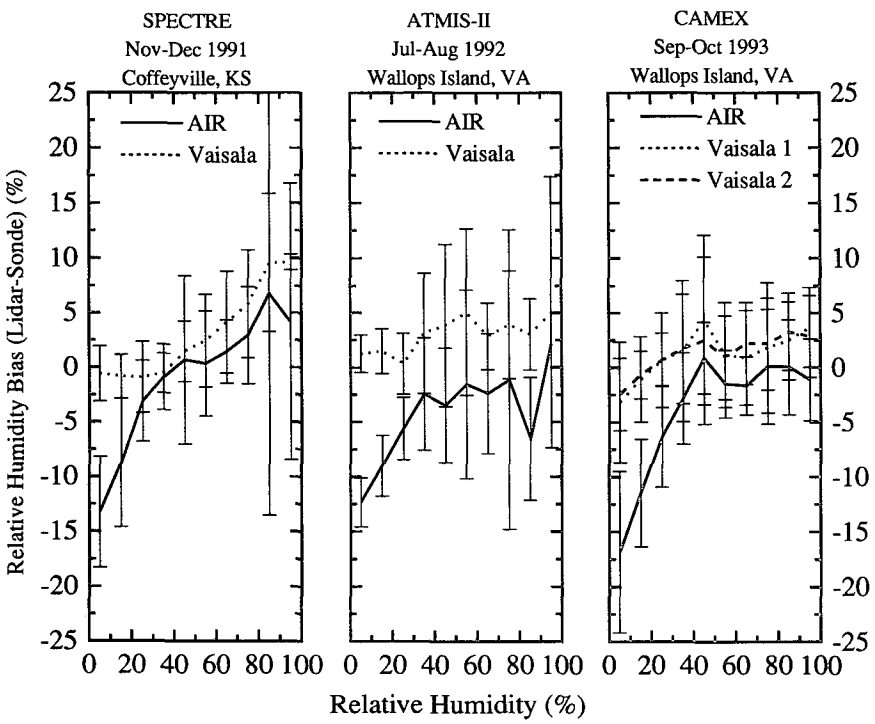

FIG. 7. Lidar–radiosonde humidity differences as a function of relative humidity for each of the three field campaigns.

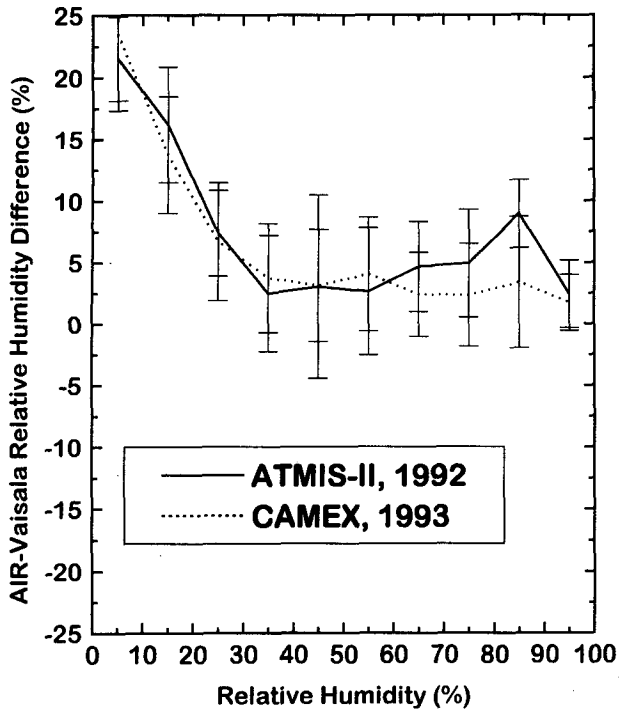

FIG. 8. AIR–Vaisala relative humidity differences for the ATMIS II and CAMEX field experiments. There were 15 joint comparisons during ATMIS II in 1992 and 24 during CAMEX in 1993.

nificantly different from 0% at the 90% confidence level. The reason for the larger AIR–Vaisala bias during the ATMIS II experiment appears related to the AIR measurements. Recall Fig. 3, which shows the lidar calibration constant computed using the AIR data during ATMIS II, was also larger than during the prior SPECTRE experiment and during the subsequent CAMEX experiment. Since the Vaisala tends to report slightly smaller relative humidities than the AIR sonde, one might expect a smaller number of high (i.e., >90%) relative humidities as measured by the Vaisala than by the AIR. Figure 6 shows some indication of this although perhaps not as clearly as expected since these data were collected during predominantly cloud-free conditions.

The differences between the lidar-derived relative humidities and those measured by the AIR and Vaisala radiosondes were also computed as a function of altitude. These results are shown in Fig. 9 as bias (lidar minus radiosonde) differences and in Fig. 10 as root-mean-square differences. The results shown were averaged over 1-km-wide bins in order to increase statistical significance. The bias and root-mean-square errors between the lidar and Vaisala are generally less than 5% for altitudes below 8 km, while the corresponding errors between the lidar and AIR sondes are less than 10%. Since these results were computed using data from all relative humidities, the higher differences between the lidar and AIR measurements are to be expected due to the inability of the algorithm associated with the carbon hygristor to report low relative humidities. Restricting the relative humidity range to values above 30% reduces the differences between the lidar and AIR humidities. Figure 11 shows a bias comparison plot computed for the CAMEX dataset using a subset of relative humidities above 30%. In this case, the bias errors between the lidar and AIR sonde are generally less than 5% for altitudes below 7 km. Figures 9 and 10 also show the excellent agreement between the two Vaisala sondes launched simultaneously about 5 km apart during the CAMEX experiment. These results indicate that at least during this experiment, differences among the coincident lidar and radiosonde water vapor profiles caused by the lidar and radiosondes sampling different atmospheric paths should be minimal.

Figures 9, 10, and 11 also give some indication of the performance of the lidar in measurement of water vapor in the upper troposphere. Since the lidar data used in these comparisons with radiosondes were 10-min sums with 75-m vertical resolution, upper-tropospheric performance is not optimal, as will be discussed in the next section. These temporal and spatial averages were used to optimize the lidar retrievals in the lower and middle troposphere where radiosonde performance is best and therefore where the lidar calibration performance could be most effectively examined. Bias trends between the lidar and radiosonde profiles in the upper troposphere can still be studied since increasing the spatial and temporal averaging of the lidar profiles simply reduces the random error and does not appreciably change the shape of the profile. As shown in Fig. 9, the lidar relative humidities tend to be somewhat greater than those reported by the Vaisala sondes and, to a lesser extent, by the AIR sondes. Because of the dry conditions and the low relative humidity problems associated with the AIR carbon hygristor discussed above, the smaller differences computed using the AIR data are to be expected. The thermal lag of the carbon hygristor element produces errors in the relative humidity values associated with cold, upper-tropospheric temperatures. Brousaides and Morrissey (1971) found that the relative humidity errors associated with the thermal lag of the carbon hygristor range from 3% in the 1013–701-mb layer to 9% in the 350–250-mb layer. The carbon hygristor is about 1°–2°C warmer than the environment due to this thermal lag (Wade and Wolfe 1989); these temperature errors would result in the AIR sensor reporting relative humidities that significantly underestimate the true values. The thermal lag characteristics of the Vaisala sensor are not well known.

The differences in the relative humidities measured by the lidar and radiosondes were computed as a function of temperature to examine potential thermal effects. These differences are shown in Fig. 12 for each

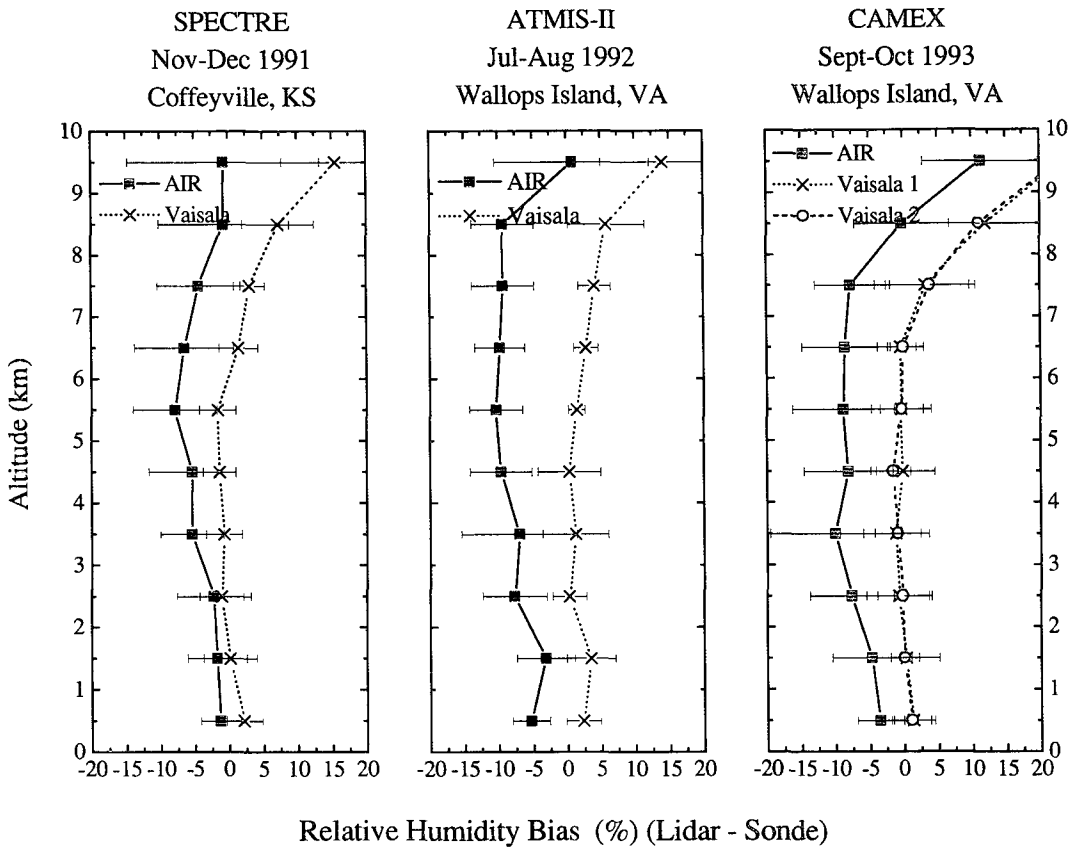

FIG. 9. Lidar–radiosonde relative humidity differences computed as a function of altitude for each of the three field experiments. The results shown were averaged over 1-km-wide bins to increase statistical significance.

of the three field campaigns. The mean differences were computed for radiosonde temperatures between −50° and 30°C in 10°C increments. The 1993 data acquired at Wallops Island and, to a lesser extent, the 1991 data acquired near Coffeyville show the lidar–radiosonde humidity differences increase slightly with decreasing temperature for temperatures below about −30°C. During CAMEX in 1993, the few temperatures below −30°C were confined to altitudes between 7 and 8 km; during SPECTRE in 1991, temperatures below −30°C occurred as low as 5 km. These differences suggest that the radiosonde humidity sensors underestimate relative humidities for these cold temperatures. Soden et al. (1994) examined the upper-tropospheric water vapor amounts obtained from the GOES 6.7-μm channel and compared these with Vaisala sondes. The Vaisala data showed a slight systematic dry bias in upper-tropospheric relative humidity as compared to the GOES data. Jackson and Gasiewski (1994) used Vaisala temperature and humidity data to compute microwave brightness temperatures and compared these with the brightness temperatures measured by the six-channel GSFC millimeter-wave imaging radiometer (MIR) flown onboard the ER-2. Comparisons of microwave brightness temperatures between the MIR and those computed using Vaisala sondes showed much better agreement than those computed using AIR sondes; these differences again attributed to the AIR sonde's poor low relative humidity reports. Jackson and Gasiewski (1994) concluded that the Vaisala measured slightly smaller amounts of water vapor than the MIR, although these differences were actually greater for the lower troposphere.

The bias and root-mean-square differences between the lidar and Vaisala relative humidities shown in Figs. 9–11 show, in each case, that the lidar profiles become increasingly moister than the Vaisala profiles above about 7.5–8 km. This difference, which increases from less than 5% at 7 km to approximately 20% at 9.5 km, may be due to both overestimation of the humidity by the lidar and underestimation by the Vaisala radiosonde. The lidar overestimation was believed to stem from signal-induced noise (SIN) in the photomultipliers used during these experiments. This noise adds an additional component to the signal that can become a significant fraction of the total signal for long ranges (Iikura et al. 1987; Lee et al. 1989). This effect, when present, affects the water vapor signals in particular

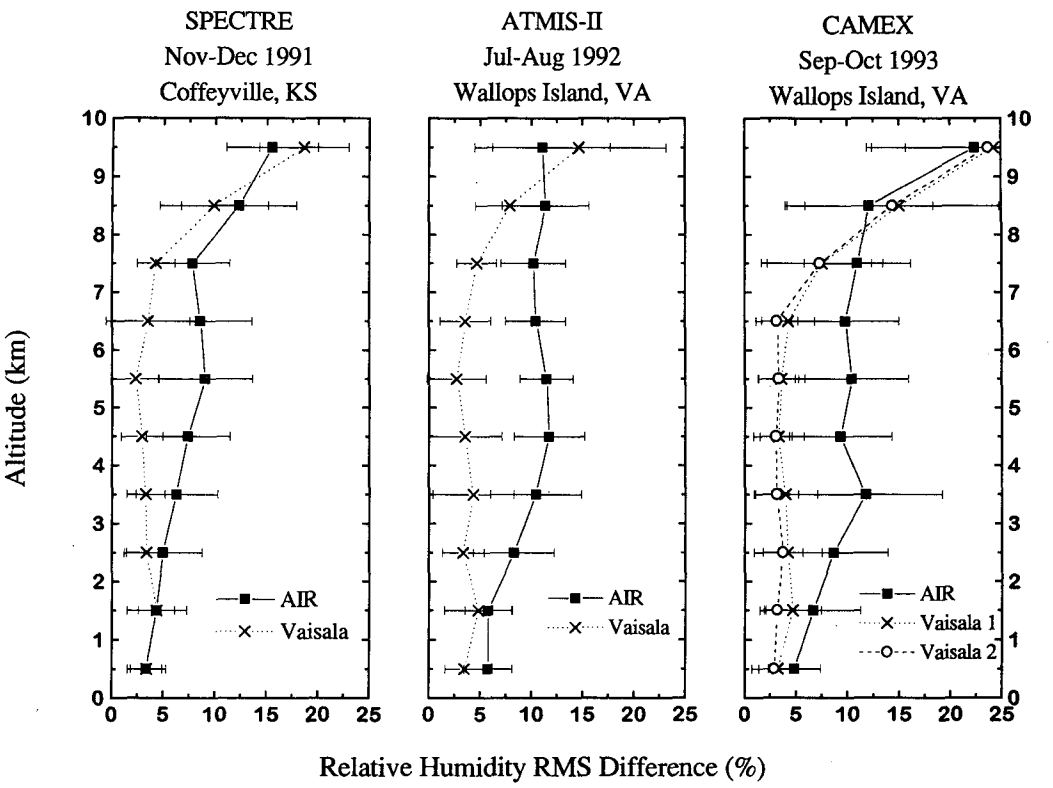

FIG. 10. Root-mean-square differences between lidar and radiosonde relative humidities as a function of altitude for each field experiment. The results shown were averaged over 1-km-wide bins to increase statistical significance.

because of the very rapid decrease in signal strength with altitude. This problem becomes apparent in locations where the Raman water vapor signal becomes small and approaches the background noise levels, such as in the dry upper troposphere or where the water vapor signal decreases abruptly due to cloud and/or aerosol attenuation. When present in the high sensitivity water vapor channel, the noise can produce overestimates of water vapor at high altitudes where the water vapor return signals are small. The bias and root-mean-square differences computed using both the AIR and Vaisala radiosondes show this trend occurred slightly during ATMIS II and to a greater extent during CAMEX. Assuming these bias trends are caused in some part by SIN, the greater evidence of this trend during the CAMEX experiment as compared to the SPECTRE experiment is likely due to the increase in atmospheric aerosol attenuation present during the experiments at Wallops Island during late summer and fall as opposed to the Coffeyville area during late fall and early winter. Increased atmospheric attenuation significantly reduces the water vapor signal so that any excess signal produced by SIN becomes much more apparent, leading to an overestimate of the derived water vapor.

We have pursued efforts similar to those described by others in an effort to reduce the influence of SIN on the lidar signals. We have used a numerical model to compute and subsequently remove the excess signal produced by SIN (Iikura et al. 1987; McDermid et al. 1990). We have not pursued this method for two reasons; it is not certain whether the excess signal can be accurately described by a simple exponential decay with time, and the method is somewhat subjective in the manner in which the coefficients used to model this decay are obtained from actual atmospheric data (McGee et al. 1991). The uncertainties associated with these assumptions can introduce significant errors in the derived water vapor amounts. Another method we have used in an attempt to reduce the effect of SIN is to measure the photomultiplier response function and to use this function in a deconvolution technique with the atmospheric signals (Sroga et al. 1983). While some improvement was realized in this effort, the reduction in SIN was insufficient to allow this technique to be used reliably with the weak Raman signals at the farthest measurement ranges; small amounts of uncorrected SIN are able to dominate the weak Raman signals at high altitudes. In addition, this method mixes noise generated by the strong, near-range signals with the weaker, far-range signals (Grund and Eloranta 1991). Because of the difficulties in trying to remove SIN during postprocessing, we have, therefore, chosen to make no effort to numerically remove SIN subse-

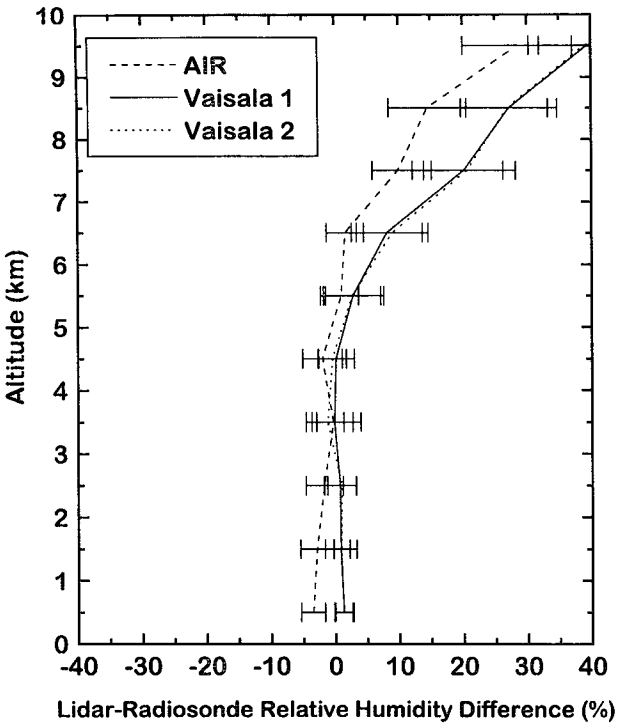

FIG. 11. Lidar–radiosonde relative humidity differences for the CAMEX experiment as a function of altitude. Unlike Fig. 9, these data are only for relative humidities above 30%.

quent to data collection. Rather, our primary effort has been to use specially selected photomultiplier tubes, which, through testing, have been shown to have low levels of excess signal associated with SIN.

7. Maximum altitude of lidar water vapor retrievals

The lidar–radiosonde comparisons presented in the previous section indicated that the difference between the lidar and radiosonde relative humidity measurements increases for altitudes above 6–8 km. In addition, the uncertainty in this difference also increases with altitude due to the increase with altitude of the random error in the lidar water vapor retrievals. Therefore, we have investigated the factors that affect the random error in the lidar water vapor retrievals. This investigation has focused on how various factors impact the retrieval of water vapor in the upper troposphere and how these effects impose a maximum altitude on the retrieved lidar water vapor profiles.

The maximum altitude of the retrieved lidar water vapor profiles under cloud-free conditions is generally determined by the size of the random error, which, in turn, depends on several instrumental and environmental factors. For a given output power and wavelength, the dominant instrumental factors include detector noise, averaging time, and vertical resolution, while the most important environmental factors are ambient water vapor concentration, background skylight, and atmospheric attenuation. We have attempted to ascertain the maximum altitude below which this lidar can retrieve water vapor profiles. Since actual data cannot easily identify how each of the above items affect upper-tropospheric water vapor measurements, we have developed a numerical model to simulate such retrievals. This model simulates the Raman water vapor and nitrogen return signals by first tracking photons through the atmosphere and instrument and then computing the number of return photons counted in each channel. Data input to the model include key system parameters, realistic atmospheric water vapor, density, and aerosol profiles, and background skylight values. The model produces simulated lidar return signals that are used exactly like actual lidar data to compute water vapor and aerosol–cloud backscattering and extinction profiles. This model has been improved over that described by Goldsmith and Ferrare (1992) in that it uses more realistic water vapor profiles as well as actual measured background skylight data.

The model was tested by determining how well the water vapor profiles generated by the simulated lidar return signals match those actually measured by the current GSFC Raman lidar. Actual water vapor profiles measured by the lidar were used as input as were the following fixed system parameters: 351-nm laser wavelength, 45-mJ laser pulse energy, 400-Hz laser repetition rate, 0.405-m^2 telescope area, 2-mrad telescope field of view, and a 2% overall system detection efficiency for the Raman water vapor signals. The background skylight signals measured by the lidar in each channel are used as are realistic aerosol and molecular attenuation profiles. These tests showed excellent agreement between measured and modeled Raman water vapor lidar profiles.

The sensitivity of the Raman lidar water vapor retrievals to changes in several system and environmental factors was modeled. The effects of changes in these factors were compared to a standard case that consisted of the following parameters: 18-W laser output power, 10-min averaging period, background skylight corresponding to a moonless night, lidar elevation at mean sea level, scan angle of 0° (zenith), 75-m vertical resolution, and boundary layer aerosol concentration corresponding to the 23-km visibility model from Shettle and Fenn (1976). The actual laser output power used for the measurements presented in this paper was slightly lower than value used in the model stated above; this difference does not significantly affect the conclusions drawn from the model results. Since the ambient water vapor concentration in the upper troposphere is highly variable and can easily vary by over an order of magnitude, it is difficult to model the lidar performance using a single water vapor profile. Therefore, four water vapor profiles were constructed and

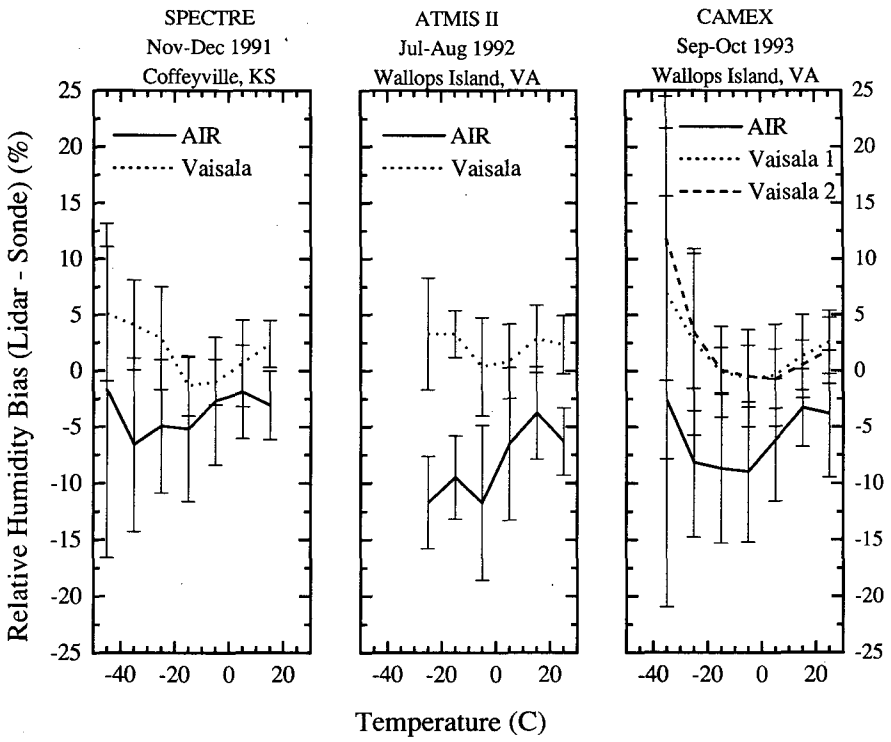

FIG. 12. Lidar–radiosonde humidity differences as a function of temperature for each of the three field campaigns.

used in the model to characterize the lidar performance under a realistic set of midlatitude atmospheric conditions. The water vapor profiles used for these models were constructed using the midlatitude summer and winter pressure and temperature profiles given by McClatchey et al. (1971). The sensitivity of the maximum altitude with respect to changes in each of these factors is shown in Fig. 13. The maximum altitude represents the altitude below which the absolute error in relative humidity is less than or equal to 10%. The most important variable is the ambient water vapor concentration, which varies by a factor of about 50 between the extreme cases shown. Integration of the water vapor profiles between the surface and selected altitudes indicates that this lidar system can normally measure water vapor profiles over an altitude region that covers approximately 99% of the total atmospheric water vapor. The effects of combining two or more factors can be roughly approximated by adding (or subtracting) the changes in altitudes shown in Fig. 13. For example, by combining the individual effects of increasing the averaging time from 10 min to 1 h and changing the vertical resolution from 75 to 300 m would increase the maximum altitude from 8.7 to about 10.3 km. This approximate additive behavior was empirically discovered when comparing the results in Fig. 13 with actual modeling runs that combined various factors. By increasing the averaging time and reducing the vertical resolution, data from this lidar system has been used to corroborate the upper-tropospheric humidity retrievals obtained from the GOES 6.7-μm channel (Soden et al. 1994).

This modeling effort did not attempt to account for an additional constraint on the upper limit of the lidar water vapor retrievals that was imposed by a limitation of the photomultiplier tubes. This limitation was believed to stem from signal-induced noise (SIN) in the photomultipliers used during this experiment. The impact of SIN on the retrieval of upper-tropospheric water vapor has been difficult to assess since we have not had the ability to compare the lidar measurements with sufficiently accurate auxiliary water vapor measurements. As was shown in section 6, radiosonde data can give only a general indication of where this problem may occur since radiosonde moisture sensors vary widely in their ability to measure water vapor in the cold, dry regions of the upper troposphere.

8. Summary and conclusions

This paper has examined the water vapor calibration characteristics of the GSFC Raman lidar during the period from 1991 to 1993, as well as the factors affecting the maximum altitude of water vapor profiles measured

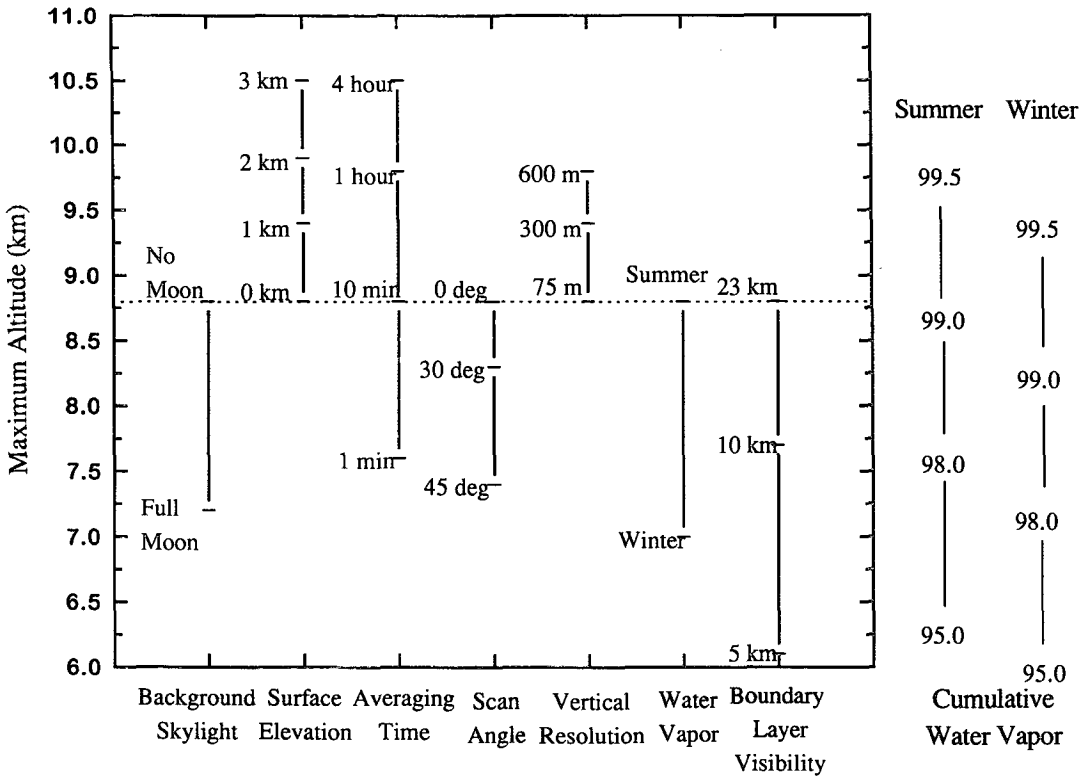

FIG. 13. Sensitivity of the maximum altitude of lidar water vapor retrievals to various instrumental and environmental factors as determined from model results. The maximum altitude represents the altitude below which the absolute error in relative humidity is less than or equal to 10%. The scales on the right show the percentage of water vapor between the surface and the given altitude for the summer and winter water vapor profiles.

by this system. A numerical model that incorporates key system and environmental parameters was used to assess the factors that affect the lidar signal to noise ratio and consequently the measurement range of the system. Using these parameters along with representative atmospheric water vapor and aerosol profiles yielded a maximum altitude of approximately 8.5 km for a 10-min, 75-m resolution profile. This altitude can be extended to about 10 km under moist conditions by reducing the temporal and spatial resolution to 1 h and 300 m, respectively. An additional factor that has limited the lidar upper-tropospheric water vapor measurements is the apparent presence of signal-induced noise in the high-sensitivity water vapor channel. Depending upon the atmospheric attenuation and the water vapor amounts, this noise source can cause the lidar to overestimate upper-tropospheric water vapor amounts above 9 km. By increasing the water vapor return signal and/or reducing the background noise at these altitudes, water vapor profiles that extend to near the tropopause can be retrieved (Bisson et al. 1994). Because of the generally poor performance of radiosonde sensors in measuring humidity in the cold, dry regions of the upper troposphere, comparisons with other humidity sensors are required to better assess the performance of the lidar and radiosondes.

The method by which the water vapor profiles produced by this lidar system are calibrated with coincident water vapor measurements is also reviewed. Water vapor profiles measured by coincident radiosondes were used to calibrate the lidar system during three experimental campaigns that occurred in 1991, 1992, and 1993. These radiosondes used the carbon hygristor resistive element as well as the thin-film capacitive element (Humicap). During this 2-yr period, the lidar calibration constant varied by less than 1% when using Vaisala data and by less than 5% when using the AIR data. In addition, these results showed that the lidar calibration differed depending on which radiosonde was used as the reference. The lidar calibration constants indicated that the thin-film capacitive elements carried by the Vaisala radiosondes reported relative humidities approximately 3%–5% lower than those reported by the carbon hygristor elements, flown in this case, by AIR radiosondes. While previous studies, as well as this paper, have noted the poor low relative humidity measurements associated with the carbon hygristor element, these systematic humidity differ-

ences between the two radiosondes were found for nearly all relative humidities above 30%. The National Weather Service is considering using Vaisala radiosondes at selected sites in the United States; thus both types of humidity sensors will be used by the NWS for routine upper-air observations (American Meteorological Society 1994). Therefore, resolving these differences in radiosonde humidity measurements will also be important in understanding the water vapor data to be acquired by the NWS radiosonde network.

Unfortunately, because it is currently not known which of the two radiosonde humidity sensors provides better overall water vapor measurements, the absolute water vapor measurement accuracy of the lidar is limited by the uncertainty introduced by these two different radiosonde humidity sensors. Attempts at reducing this uncertainty by using other water vapor measurements from microwave radiometers, satellite IR radiances measured by the GOES satellite, and coincident aircraft measurements have not yet provided definitive results. The difficulties associated with using radiosonde and other sensors to accurately calibrate the Raman lidar highlight the need for a comprehensive set of experiments to characterize these and other moisture-measuring instruments.

Acknowledgments. We wish to thank Dr. Andrew Heymsfield at the National Center for Atmospheric Research for providing the King Air measurements of water vapor acquired during the FIRE-II experiment. We also appreciate the use of the Vaisala radiosonde data acquired by Dr. William Smith and personnel from the Cooperative Institute for Meteorological Satellite Studies (CIMSS)/University of Wisconsin—Madison.

REFERENCES

American Meteorological Society, 1994: Data correction part of NWS modernization. *Bull. Amer. Meteor. Soc.*, **75,** 882.

Ansmann, A., M. Riebesell, and C. Weitkamp, 1990: Measurement of atmospheric aerosol extinction profiles with a Raman lidar. *Opt. Lett.*, **15,** 746–748.

——, ——, U. Wandinger, C. Weitkamp, E. Voss, W. Lahmann, and W. Michaelis, 1992: Combined Raman elastic-backscatter lidar for vertical profiling of moisture, aerosol extinction, backscatter, and lidar ratio. *Appl. Phys. B,* **55,** 18–28.

Arking, A., 1991: The radiative effects of clouds and their impact on climate. *Bull. Amer. Meteor. Soc.*, **71,** 795–813.

Betts, A. K., 1990: Greenhouse warming and the tropical water budget. *Bull. Amer. Meteor. Soc.*, **71,** 1464–1465.

Bisson, S. E., J. E. M. Goldsmith, and A. D. Del Genio, 1994: Measurements of upper tropospheric moisture with a Raman lidar, *17th Int. Laser Radar Conf.*, Sendai, Japan, Int. Radiation Commission.

Brousaides, F. J., 1975: The radiosonde hygristor and low humidity measurements. *Bull. Amer. Meteor. Soc.*, **56,** 229–234.

——, and J. F. Morrissey, 1971: Improved humidity measurements with a redesigned radiosonde humidity duct. *Bull. Amer. Meteor. Soc.*, **52,** 870–875.

Eichinger, W. E., D. I. Cooper, M. Parlange, and G. Katul, 1993: The application of a scanning water Raman-lidar as a probe of the atmospheric boundary layer. *IEEE Trans. Geosci. Remote Sens.*, **31,** 70–79.

Elliott, W. P., and D. J. Gaffen, 1991: On the utility of radiosonde humidity archives for climate studies. *Bull. Amer. Meteor. Soc.*, **72,** 1507–1520.

England, M. N., R. A. Ferrare, S. H. Melfi, and D. N. Whiteman, 1992: Atmospheric water vapor measurements: Comparison of microwave radiometry and lidar. *J. Geophys. Res.*, **97,** 899–916.

——, F. J. Schmidlin, and J. M. Johansson, 1993: Atmospheric moisture experiments: A microwave radiometer–radiosonde comparison. *IEEE Trans. Geosci. Remote Sens.*, **31,** 389–398.

Ferrare, R. A., D. Whiteman, and S. H. Melfi, 1990: Lidar measurements of temperature in the troposphere and lower stratosphere. *Optical Remote Sensing of the Atmosphere Technical Digest,* Vol. 4, Optical Society of America, 508–511.

——, S. H. Melfi, D. N. Whiteman, and K. D. Evans, 1992: Raman lidar measurements of Pinatubo aerosols over southeastern Kansas during November–December 1991. *Geophys. Res. Lett.*, **19,** 1599–1602.

——, ——, ——, and ——, 1993: Coincident measurements of atmospheric aerosol properties and water vapor by a scanning Raman lidar, *Optical Remote Sensing of the Atmosphere Technical Digest,* Vol. 5, Optical Society of America, 11–14.

Garand, L., C. Grassotti, J. Halle, and G. Klein, 1992: On differences in radiosonde humidity-reporting practices and their implications for numerical weather prediction and remote sensing. *Bull. Amer. Meteor. Soc.*, **73,** 1417–1423.

Goldsmith, J. E. M., and R. A. Ferrare, 1992: Performance modeling of daytime raman lidar systems for profiling atmospheric water vapor, *16th Int. Laser Radar Conf.*, Cambridge, MA, Int. Radiation Commission.

——, S. E. Bisson, R. A. Ferrare, K. D. Evans, D. N. Whiteman, and S. H. Melfi, 1994: Raman lidar profiling of atmospheric water vapor: Simultaneous measurements with two collocated systems. *Bull. Amer. Meteor. Soc.*, **75,** 975–982.

Griffin, V. L., A. R. Guillory, M. Susko, and J. E. Arnold, 1994: Operations summary for the Convection and Moisture Experiment (CAMEX). NASA TM-108445, 180 pp.

Grund, C. J., and E. W. Eloranta, 1991: University of Wisconsin high spectral resolution lidar. *Opt. Eng.*, **30,** 6–12.

Han, Y., J. B. Snider, E. R. Westwater, S. H. Melfi, and R. A. Ferrare, 1994: Observations of water vapor by ground-based microwave radiometers and Raman lidar. *J. Geophys. Res.*, **99**(D9), 18 695–18 702.

Heymsfield, A. J., and L. M. Miloshevich, 1993: Homogeneous ice nucleation and supercooled liquid water in orographic wave clouds. *J. Atmos. Sci.*, **50,** 2335–2353.

——, and ——, 1995: Relative humidity and temperature influences on cirrus formation and evolution: Observations from wave clouds and FIRE II. *J. Atmos. Sci.*, in press.

Iikura, Y., N. Sugimoto, Y. Sasano, and H. Shimzu, 1987: Improvement on lidar data processing for stratospheric aerosol measurements. *Appl. Opt.*, **26,** 5299–5306.

Ismail, S., and E. V. Browell, 1994: Recent lidar technology developments and their influence on measurements of tropospheric water vapor. *J. Atmos. Oceanic Technol.*, **11,** 76–84.

Jackson, D. M., and A. J. Gasiewski, 1994: Millimeter-wave radiometric observations of the troposphere: A comparison of measurements and calculations based on radiosonde and Raman lidar. *IEEE Trans. Geosci. Remote Sens.*, in press.

Kaiser, J. F., and W. A. Reed, 1977: Data smoothing using low-pass digital filters. *Rev. Sci. Instrum.*, **48,** 1447–1457.

Keckhut, P., M. L. Chanin, and A. Hauchecorne, 1990: Stratospheric temperature measurement using Raman lidar. *Appl. Opt.*, **29,** 5182–5186.

Koch, S. E., P. B. Dorian, R. Ferrare, S. H. Melfi, W. C. Skillman, and D. Whiteman, 1991: Structure of an internal bore and dis-

sipating gravity current as revealed by Raman lidar. *Mon. Wea. Rev.*, **119**, 857–887.

Larsen, J. C., E. W. Chiou, W. P. Chu, M. P. McCormick, L. R. McMaster, S. Oltmans, and D. Rind, 1993: A comparison of the stratospheric aerosol and gas experiment II tropospheric water vapor to radiosonde measurements. *J. Geophys. Res.*, **98**(D3), 4897–4917.

Lee, H. S., G. K. Schwemmer, C. L. Korb, M. Dombrowski, and C. Prasad, 1989: Gated photomultiplier response characterization for DIAL measurements. *Appl. Opt.*, **29**, 3303–3315.

Lindzen, R. S., 1990: Some coolness concerning global warming. *Bull. Amer. Meteor. Soc.*, **71**, 288–299.

List, R. J., 1949: *Smithsonian Meteorological Tables*. 6th ed. Smithsonian Institution Press, 527 pp.

McClatchey, R. A., R. W. Fenn, J. E. A. Selby, F. E. Volz, and J. S. Garing, 1971: Optical properties of the atmosphere (Revised), Environmental Research Papers, No. 354, AFCRL-71-0279, Air Force Cambridge Research Laboratories.

McDermid, I. S., S. M. Godin, and L. O. Lindqvist, 1990: Ground-based laser DIAL system for long-term measurements of stratospheric ozone. *Appl. Opt.*, **29**, 3603–3612.

McGee, T. J., D. Whiteman, R. Ferrare, J. J. Butler, and J. F. Burris, 1991: STROZ LITE: Stratospheric ozone lidar trailer experiment. *Opt. Eng.*, **30**, 31–39.

Melfi, S. H., and D. N. Whiteman, 1985: Observation of lower atmospheric moisture structure and its evolution using a Raman lidar. *Bull. Amer. Meteor. Soc.*, **66**, 1282–1292.

——, ——, and R. Ferrare, 1989: Observation of atmospheric fronts using Raman lidar moisture measurements. *J. Appl. Meteor.*, **28**, 789–806.

Pratt, R. W., 1985: Review of radiosonde humidity and temperature errors. *J. Atmos. Oceanic Technol.*, **2**, 404–407.

Ramanathan, V., 1988: The greenhouse theory of climate change: A test by an inadvertent global experiment. *Science*, **240**, 293–299.

Schmidlin, F. J., 1988: WMO international radiosonde comparison, phase II final report, 1985. Instruments and observing methods report, No. 29 WMO/TD No. 312, WMO, Geneva, Switzerland, 113 pp.

Shettle, E. P., and R. W. Fenn, 1976: Models of the atmospheric aerosols and their optical properties. *Proc. AGARD Conf. No. 183, Optical Propagation in the Atmosphere.* Presented at the Electromagnetic Wave Propagation Panel Symposium, Lyngby, Denmark, AGARD-CP-183, ADA028-615, 1976.

Soden, B. J., S. A. Ackerman, D. O'C. Starr, S. H. Melfi, and R. A. Ferrare, 1994: Comparison of upper tropospheric water vapor from GOES, Raman lidar, and CLASS measurements during FIRE-II. *J. Geophys. Res.*, **99**(D10), 21 005–21 016.

Sroga, J. T., E. W. Eloranta, S. T. Shipley, F. L. Roesler, and P. J. Tryon, 1983: High spectral resolution lidar to measure optical scattering properties of atmospheric aerosols. Part 2: Calibration and data analysis. *Appl. Opt.*, **22**, 3725–3732.

Starr, D. O'C., 1994: Water vapor measurements and the GEWEX Water Vapor Project (GVaP) Pilot Phase Instrument Intercomparison Campaign., Preprints, *Fifth Symp. on Global Change Studies*, Nashville, TN, Amer. Meteor. Soc., 199–202.

——, and S. H. Melfi, 1991: The role of water vapor in climate: A strategic research plan for the proposed GEWEX water vapor project (GVaP). NASA Conf. Publication, CP3120, NASA, Washington, DC, 50 pp.

Twomey, S., 1991: Aerosols, clouds, and radiation. *Atmos. Environ.*, **25A**, 2435–2442.

Vaughan, G., D. P. Waring, L. Thomas, and V. Mitev, 1988: Humidity measurements in the free troposphere using Raman backscatter. *Quart. J. Roy. Meteor. Soc.*, **114**, 1471–1484.

Wade, C. G., 1994: An evaluation of problems affecting the measurement of low relative humidity on the United States radiosonde. *J. Atmos. Oceanic Technol.*, **11**, 687–700.

——, and D. E. Wolfe, 1989: Performance of the VIZ carbon hygristor in a dry environment, Preprints, *12th Conf. on Weather Analysis and Forecasting*, Monterey, CA, Amer. Meteor. Soc., 58–62.

Wang, J. R., S. H. Melfi, P. Racette, D. N. Whiteman, L. A. Chang, R. A. Ferrare, K. D. Evans, and F. J. Schmidlin, 1995: Simultaneous measurements of atmospheric water vapor with MIR, Raman lidar, and rawinsondes. *J. Appl. Meteor.*, **34**, 1595–1607.

Westwater, E. R., M. J. Falls, and I. A. Popa Foting, 1989: Ground-based microwave radiometric observations of precipitable water vapor: A comparison with ground truth from two radiosonde observing systems. *J. Atmos. Oceanic Technol.*, **6**, 724–730.

Whiteman, D. N., S. H. Melfi, and R. A. Ferrare, 1992a: Raman lidar system for the measurement of water vapor and aerosols in the earth's atmosphere. *Appl. Opt.*, **31**, 3068–3082.

——, and Coauthors, 1992b: Advanced Raman water vapor lidar, *16th Int. Laser Radar Conf.* (NASA Conference Publication 3158, part 2) 483–484.